Chemically Modulated Band Gap in Bilayer Graphene Memory Transistors with High On/Off Ratio

Si Young Lee,[†,§] Dinh Loc Duong,[†,¶] Quoc An Vu,[†,‡] Youngjo Jin,[†,‡] Philip Kim,[§] and Young Hee Lee[*,†,‡]

[†]Center for Integrated Nanostructure Physics (CINAP), Institute for Basic Science (IBS), and [‡]Department of Energy Science, Department of Physics, Sungkyunkwan University, Suwon 440-746, Republic of Korea and [§]Department of Physics, Harvard University, Cambridge, Massachusetts 02138, United States
[¶]Present address: Max Planck Institute for Solid State Research, Heisenbergstrasse 1, D-70569 Stuttgart, Germany.

ABSTRACT

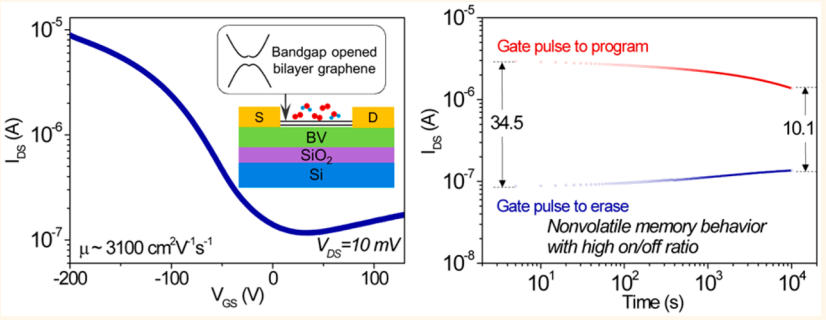

We report a chemically conjugated bilayer graphene field effect transistor demonstrating a high on/off ratio without significant degradation of the on-current and mobility. This was realized by introducing environmentally stable benzyl viologen as an electron-donating group and atmospheric dopants as an electron-withdrawing group, which were used as dopants for the bottom and top of the bilayer graphene, respectively. A high mobility of ~3100 $cm^2 V^{-1} s^{-1}$ with a high on/off ratio of 76.1 was obtained at room temperature without significant degradation of the on-current. This is attributed to low charge scattering due to physisorbed dopants without provoking sp^3 structural disorders. By utilizing our band-gap-opened bilayer graphene, excellent nonvolatile memory switching behavior was demonstrated with a clear program/erase state by applying pulse gate bias. The initial program/erase current ratio of ~34.5 was still retained at higher than 10 even after 10^4 s.

KEYWORDS: bilayer graphene · band-gap opening · doping · on/off ratio · nonvolatile memory

The massless Dirac particle feature in graphene shows an extremely high carrier mobility and has led to numerous scientific[1−4] and technological breakthroughs.[5−7] Although high-frequency devices exhibit excellent frequency characteristics up to 300 GHz,[8] applications in switching devices such as transistor-type memory devices and logic circuits suffer from a low on/off ratio, typically less than 10, due to the intrinsically metallic feature of graphene.[9−12] The poor on/off ratio originates from the absence of an electronic band gap. Therefore, opening the band gap in graphene remains a major hurdle in fundamental research.

The band gap of graphene has been created by narrowing the channel width (<10 nm), which induces the quantum confinement effect.[13,14] A graphene nanoribbon field effect transistor (FET) exhibits a high on/off ratio (<10^6) at room temperature. However, the carrier mobility (~200 $cm^2 V^{-1} s^{-1}$) was significantly degraded by edge scattering and, in addition, the fabrication process is not technologically scalable. Band-gap opening in Bernal-stacked bilayer graphene was also demonstrated by applying a perpendicular electric field, which results in the breaking of inversion symmetry between the two layers.[15−17] This was realized by applying a high bias on the top and bottom gates in the bilayer graphene FET, and an on/off ratio of 10^2 was reported at room temperature.[16] This method is highly advantageous for large-scale integration compared to the

* Address correspondence to (Y. H. Lee) leeyoung@skku.edu.

Received for review May 24, 2015 and accepted August 26, 2015.

Published online August 26, 2015
10.1021/acsnano.5b03130

graphene nanoribbon FET. However, the dual-gate structure is undesirable from a technological point of view. Dual-side chemical doping on bilayer graphene was proposed to generate a perpendicular electric field with a single gate.[18−21] Several theoretical calculations predicted high band-gap opening (~350 meV) with n-type and p-type doping on opposite sides of bilayer graphene.[20,21] However, the reported on/off ratio of this graphene FET was less than 26 with a measured optical band gap of 210 meV (larger than the electrical band gap of 124 meV).[18] Yet, it has been estimated that a band gap of 350 meV is needed to maintain an on/off ratio of 10^3.[22] This discrepancy is attributed to the use of ineffective dopants or doping level control only on one side of graphene, which generates a relatively low electric field across bilayer graphene, which is not sufficient to break the inversion symmetry. Moreover, the on-current and mobility (~800 $cm^2\ V^{-1}\ s^{-1}$) are significantly reduced due to impurity scattering introduced by the dopants.[18]

The strategy employed in this study was to introduce simple chemical doping on both sides of bilayer graphene to break the inversion symmetry and open the band gap of bilayer graphene without introducing a complicated double-gate structure. One key element of this is the choice of chemical dopant to minimize charge scattering so as to maintain the on-current and mobility. Here, we chose environmentally stable benzyl viologen (BV) as an electron-donating group at the bottom of bilayer graphene, which is also used as a trap layer for nonvolatile memory devices. Atmospheric dopants such as oxygen and moisture as an electron-withdrawing group were used as dopants for the top of bilayer graphene. Because both dopants are physisorbed on the surface of bilayer graphene without provoking sp^3 structural disorders, charge scattering is minimized to maintain the on-current and mobility. Different doping concentrations were evaluated to control the electric field across bilayer graphene. Nonvolatile memory behavior was successfully demonstrated from the FET with the band-gap-opened bilayer graphene channel.

RESULTS AND DISCUSSION

Figure 1a depicts the principle of band-gap opening in bilayer graphene using dual-side conjugation of molecular dopants. The bottom side of bilayer graphene is doped by an n-type dopant (BV), and the top side is doped by a p-type dopant (atmospheric molecules such as oxygen and moisture). Electrons are donated from BV to the bottom graphene layer, while electrons are withdrawn from the top graphene layer to atmospheric dopants. As a result, a strong local electric field is generated by positive and negative charges located on two opposite sides of the molecules, resulting in breaking of the inversion symmetry and opening of the band gap in bilayer graphene. A schematic and optical image of a bilayer graphene FET are shown in Figure 1b and c, respectively. The environmentally stable BV layer was spin-coated on the SiO_2 (300 nm)/Si wafer, and then bilayer graphene was exfoliated on the BV layer by the Scotch tape method. The roughness of BV was very small (~0.17 nm) due to the high spin-coating speed (see Supporting Information Figure S1a and b). The source and drain electrodes were formed by e-beam/thermal evaporation of Cr/Au (5/70 nm) using a TEM grid as a shadow mask. Finally, the top of bilayer graphene was naturally p-type doped by the atmospheric dopants present in air. The experimental details are shown in Supporting Information Figure S2.

The bottom doped graphene was studied by Raman spectroscopy with 2.41 eV excitation (Figure 1d). Due to the BV layer (10 mM), the G-band was shifted toward a higher wavenumber compared to that of pristine graphene (~1580 cm^{-1})[23] and the intensity of the G/2D ratio was increased for both monolayer and bilayer graphene.[24] The difference in the Raman shift between monolayer and bilayer graphene is that the peak position of the G-band of monolayer graphene (~1594 cm^{-1}) is shifted more than that of bilayer graphene (~1588 cm^{-1}). In addition, the G-band of monolayer graphene can be fit with one Lorenzian peak, while that of bilayer graphene is fit with at least two Lorenzian peaks. This splitting of the G-band in bilayer graphene comes from the different doping levels between the top and bottom graphene layers.[25,26] It is important to note that there is no D-band generated by doping in either monolayer or bilayer graphene, implying that BV molecules do not generate any sp^3-like structural disorder in graphene, as shown in the insets of Figure 1d. The Raman spectra of the thicker layers were also investigated, approaching those of pristine values due to the minimized doping effect (see Supporting Information Figure S3). Figure 1e shows the $I_{DS}-V_{GS}$ transfer curve of the bottom-doped bilayer graphene FET with 10 mM BV on a SiO_2/Si wafer under ambient conditions. Due to electron donation from the BV layer to graphene, the charge neutrality point (CNP) of bilayer graphene is shifted toward the negative gate voltage, indicating that n-type doping is effective. A large hysteresis originates mainly from trapped charges in the BV layer, which is not observed in the graphene FET fabricated on SiO_2 (300 nm)/Si wafer.[27]

The effects of dual-side doping in a bilayer graphene FET are electrically characterized at room temperature in Figure 2. First, a bilayer graphene FET doped with 10 mM BV was measured under high vacuum (~10^{-6} Torr) to eliminate the effect of atmospheric molecules on the top of graphene (black curve in Figure 2a). The $I_{DS}-V_{GS}$ measurement indicates n-type behavior of the FET with an on/off ratio of 4.9 and a V_{CNP} at a high negative voltage of −168 V. This result confirms that the Fermi level of bilayer graphene is shifted toward

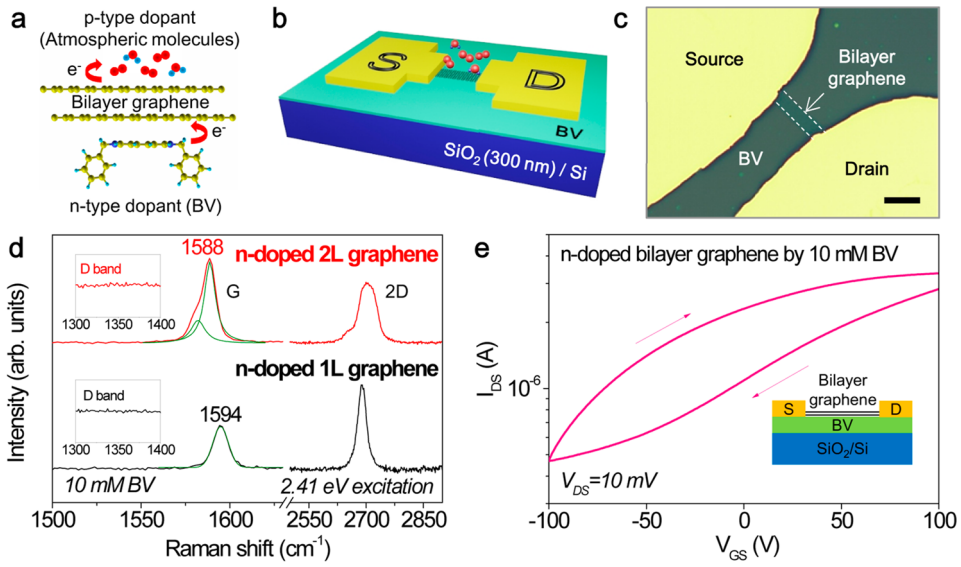

Figure 1. (a) Principle of band-gap opening of bilayer graphene by chemical doping with n-type (BV) and p-type dopants (O_2, H_2O) on opposite sides of the bilayer graphene. (b) Schematic of the dual-side doped bilayer graphene FET on a SiO_2/Si substrate. Atmospheric dopants (O_2, H_2O) are located on the bilayer graphene. (c) Optical image of the fabricated FET with a bilayer graphene channel, source, and drain on the BV layer. Scale bar: 10 μm. (d) Raman spectra of monolayer and bilayer graphene on 10 mM BV with 2.41 eV excitation, showing the G-band (fitted with Lorenzian peaks) and 2D-band. The D-bands are shown in the insets. (e) Initial $I_{DS}-V_{GS}$ transfer curve of the bottom-doped bilayer graphene FET by 10 mM BV with V_{DS} = 10 mV.

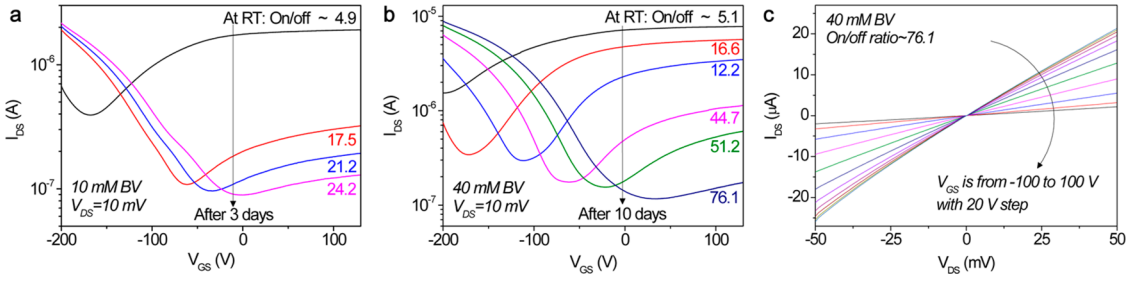

Figure 2. $I_{DS}-V_{GS}$ transfer curves of bilayer graphene FETs at room temperature with (a) 10 mM BV and (b) 40 mM BV on the bottom of bilayer graphene where a V_{DS} of 10 mV was applied. V_{GS} was swept from −200 to 130 V. (c) $I_{DS}-V_{DS}$ characteristics of the bilayer graphene FET with 40 mM BV. The curves were measured when the on/off ratio of the FET was 76.1 and the V_{GS} was swept from −100 to 100 V with 20 V steps.

the conduction band, and therefore, the BV doping is effective. To dope the top of bilayer graphene with p-type dopants, the FET was held under ambient conditions. The p-type doping is contributed by atmospheric dopants such as oxygen or moisture, which have been used as effective p-type dopants for graphene.[28] After 1 day, the $I_{DS}-V_{GS}$ measurement reveals that the FET shows p-type behavior with an improved on/off ratio of 17.5 and a V_{CNP} at −60 V, implying that the Fermi level is shifted down to the valence band and the local electric field generated by the n- and p-type dopants opens the band gap of bilayer graphene. The on/off ratio is further increased to 24.2 and the V_{CNP} is shifted toward a positive gate voltage by keeping the device under ambient conditions for 3 days. To enhance the local electric field between two opposite dopants, we used a higher concentration of 40 mM BV (Figure 2b). The $I_{DS}-V_{GS}$ transfer curve measured under a high vacuum (~10^{-6} Torr) reveals a similar on/off ratio of ~5.1, while the V_{CNP} shifted more toward a negative value because of the stronger n-type doping effect (black curve in Figure 2b). The on/off ratio gradually increases and the V_{CNP} is shifted toward a positive value as the p-type doping concentration increases by keeping the FET in air. After 10 days, the on/off ratio increased significantly up to 76.1, which is more than 10 times higher than that of graphene FET without band-gap opening. The tendency of the changes of the transfer curves is similar to the FET with 10 mM BV, while the magnitude of the changes is different. To the best of our knowledge, this on/off ratio is the highest value among reports of a chemically opened band gap in a bilayer graphene FET without a double-gate structure at room temperature.[18,25,29] We compared the p-type doping effect with high-purity O_2 gas (see Supporting Information Figure S4). First, we measured $I-V$ characteristics of our device after fabrication in air. Our device was then installed in the vacuum chamber and characterized again. The device was recovered to the original

n-type after vacuum ($\sim 10^{-6}$ Torr). In other words, the p-type doping effect (by atmospheric dopants) was minimized. Our device was again electrically characterized by introducing high-purity oxygen in the chamber. As the oxygen content increased, the off-current was slightly decreased with consistent threshold voltage shift to the right side, increasing the p-region. This trend is similar to that with atmospheric dopants. However, the off-current with atmospheric dopants was more severely reduced in the case of air doping. This difference results from the absence of moisture and corresponds to the G-band shift of the Raman spectra.[28] Figure 2c shows the $I_{DS}-V_{DS}$ characteristics of the FET shown in Figure 2b with an on/off ratio of 76.1. The transfer curves are linear, indicating that ohmic contacts between the electrodes and bilayer graphene are formed and the current is clearly modulated by the gate voltage.

The effects of atmospheric doping on the properties of a bilayer graphene FET are shown as a function of the V_{CNP} shift in Figure 3. As shown in the electrical characteristics in Figure 2a and b, the shift of V_{CNP} toward a positive gate voltage indicates the degree of p-type doping (atmospheric doping). Plots of V_{CNP} *versus* the maximum current (I_{ON}) and minimum current (I_{OFF}) and their ratios extracted from the $I_{DS}-V_{GS}$ transfer curves are shown in Figure 3a and b. As V_{CNP} shifts toward the positive gate voltage, I_{ON} is maintained without much change for both 10 and 40 mM BV, implying that atmospheric dopants do not degrade the quality of bilayer graphene. On the other hand, I_{OFF} gradually decreases, indicating that a stronger local electric field is generated and, thus, a large band gap is opened. As a result, the on/off ratio increased effectively to 24.2 for 10 mM BV and 76.1 for 40 mM BV.

In Figure 3c and d, the field effect mobilities of both electrons and holes are determined by applying the equation $\mu = (Lg_m)/(WC_{OX}V_{DS})$, where L is the channel length, g_m $(=dI_{DS}/dV_{GS})$ is the maximum transconductance, W is the channel width, C_{OX} is the gate capacitance per unit area from BV/SiO_2 (see Supporting Information Figure S1), and V_{DS} is the applied source–drain voltage. When the FET is evaluated under high vacuum, the electron mobility (~ 1500 cm^2 V^{-1} s^{-1}) is high due to electron transfer from BV to graphene, while the hole mobility is very low. As V_{CNP} shifts toward the positive gate voltage, the electron mobility decreases, while the hole mobility increases up to ~ 3100 cm^2 V^{-1} s^{-1} for both 10 and 40 mM BV, resulting from the accumulation of atmospheric dopants. The maximum electron mobility is lower than the maximum hole mobility. This can be explained by the dominant electron (majority) scattering in the n-region, while hole scattering is reduced due to the charge compensation by electrons in the p-region. Figure 3e shows the effect of atmospheric doping on the Raman spectra. The G-band and intensity of the G/2D ratio of bilayer graphene after exfoliation on 10 mM BV are recovered to close to those of pristine bilayer graphene after exposing the FET to air for 5 days. This indicates that the donated and extracted electrons are redistributed and compensated in the bilayer graphene. The D-band does not appear in the Raman spectra even after 5 days, as shown in the inset in Figure 3e. Because electron–phonon interactions in graphene are weak, no structural disorder-related sp^3 hybridization occurs, even with possible local charge redistribution near the dopants.

In Figure 3f, the electrical band gap is calculated by assuming that twice of Schottky barrier height at CNP is the band gap of the bilayer graphene.[16] The band gap can be computed as $\Delta E_g = 2\Delta\varphi_{barrier} = 2(k_BT/q)\ \ln(I^0_{off}/I_{off})$, where ΔE_g is the increased band gap, $\Delta\varphi_{barrier}$ is the difference of the Schottky barrier heights before and after band-gap opening, k_B is the Boltzmann constant, T is temperature, I^0_{off} is the off-current when the band gap is zero, and I_{off} is the off-current after band-gap opening. Here, I^0_{off} is obtained from the transfer curve measured under high vacuum (black curves in Figure 2a and b) because the on/off ratio is similar to that of a pristine graphene FET. ΔE_g is equal to E_g in our case, since the band gap of each transfer curve is calculated based on the same I^0_{off}. The calculated band gap increases as the V_{CNP} shifts toward a positive gate bias, demonstrating that a higher band gap can be achieved with a higher p-type concentration. Overall, the trend of the band-gap increase is similar for different BV concentrations, while the band gap with 40 mM BV is larger than that obtained with 10 mM BV. The obtained maximum band gap is 77 meV with 10 mM BV. This further increased up to 132 meV with the 40 mM BV concentration. According to previous reports, the calculated band-gap values are smaller than the optically measured band gap[15,16,18] and comparable with the band gap obtained by low-temperature measurement.[16] It was not possible for our device to measure the band gap by low-temperature or optical measurement due to the desorption of atmospheric molecules from the top of bilayer graphene in a vacuum and the small graphene flake size. Therefore, we expect that the calculated electrical band gap in our article is still reliable, since the band gap is comparable with the one obtained by low-temperature measurement, as reported previously.[16]

To understand how the band gap opens in our experiments, we performed a simulation using density functional theory with the Dmol3 package (Figure 4). The model consists of 144 carbon atoms in the supercell. BV and O_2 molecules are adsorbed on opposite sides of the bilayer graphene. The whole structure was optimized until the atomic forces on the atoms were smaller than 0.02 eV/Å. Details of the calculated parameters can be found in our previous work.[19] When the bilayer graphene is doped by only BV (Figure 4a), an

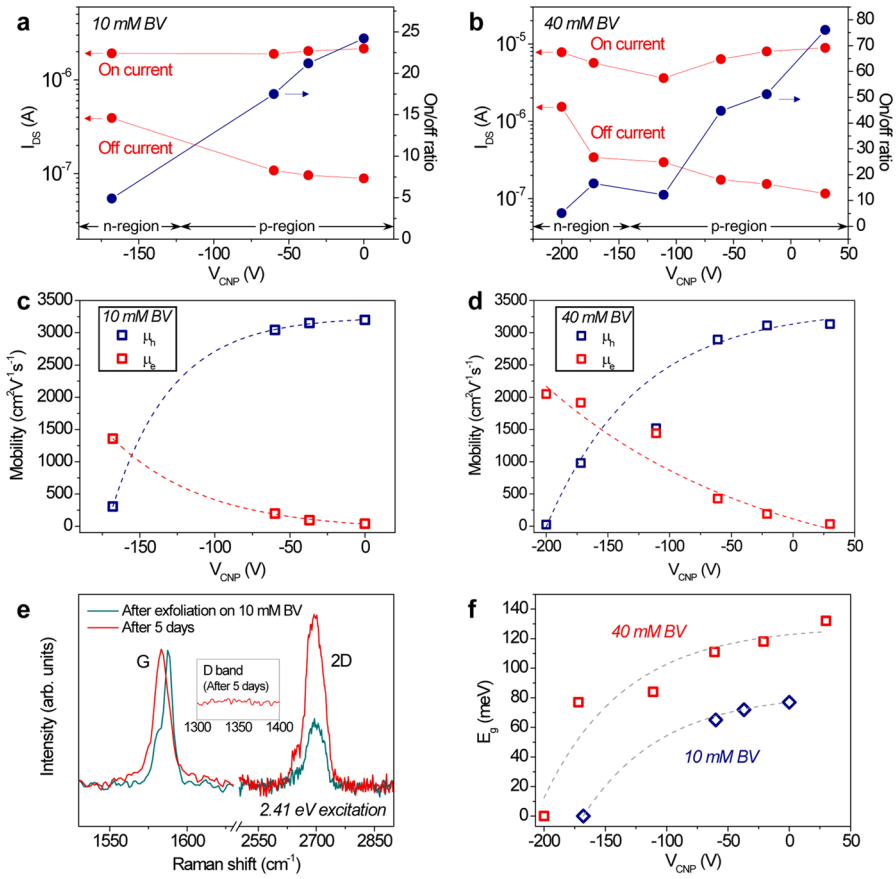

Figure 3. On-current, off-current, and on/off ratio of the FET with (a) 10 mM and (b) 40 mM BV as a function of the V_{CNP}. Field effect mobilities of the electrons and holes of the FET with (c) 10 mM and (d) 40 mM BV. The dotted lines are the fit of the data. (e) Changes in the Raman spectra of bilayer graphene with 10 mM BV after exfoliation and after 5 days of holding under ambient conditions, showing G- and 2D-bands. The D-band obtained after 5 days is shown in the insets. (f) Calculated electrical band gaps with 10 and 40 mM BV. The dotted lines are the fit of the data.

electron is transferred from BV to graphene and the Fermi level is pushed into the conduction band. This is equivalent to heavy n-type doping or a degenerate semiconductor due to the high BV concentration used in the calculations. It is clearly shown that electrons are accumulated on graphene (blue color), while they are depleted in the BV molecules (yellow color). The band gap is opened to 164 meV. In the case of O_2 (Figure 4b), electrons are extracted from graphene to O_2 and the Fermi level is shifted toward the valence band. A small band gap of 162 meV is opened by doping with individual O_2 molecules. The band gap increases up to 301 meV when BV and O_2 molecules are combined together on the bottom and top of bilayer graphene. The band gap is further opened to 352 meV when two O_2 molecules are introduced on the top of bilayer graphene. It is of note that the Fermi level position can be shifted up or down depending on the relative concentration of both dopants. In Figure 4c, the Fermi level is still located near the conduction band edge due to the high n-type doping of BV, while it is down-shifted with increasing O_2 concentration, as shown in Figure 4d. This trend is consistent with our experimental results, although the extracted experimental electrical band gap is smaller than the simulation result. This discrepancy originates from the gap states created by BV and O_2. These gap states are generated by the charge transfer between dopants and graphene, in other words, the work function modulation of graphene, not by the sp^3 hybridization with graphene layers. They are the sources of leakage current, increasing the off-current. In addition, the gap states can provoke charge scattering, slightly decreasing the on-current. This reduces the effective electrical band gap in the O_2/BV-doped samples.

In our simulation, the gap states are quite dispersed because of the high doping concentration, resulting from the small unit cell size of 14.4 Å. At high doping concentration, the dopants between unit cells are not completely isolated. As a consequence, interactions between dopants are created, forming a dispersed band or delocalized states. However, we believe that the dispersion of doping states is smaller if we simulate with a bigger cell size. Unfortunately, we could not increase the size of the unit cell due to our limitation of computational resources. In real experiments, the doping concentration could be lower than that in our simulation because BV molecules are not well aligned

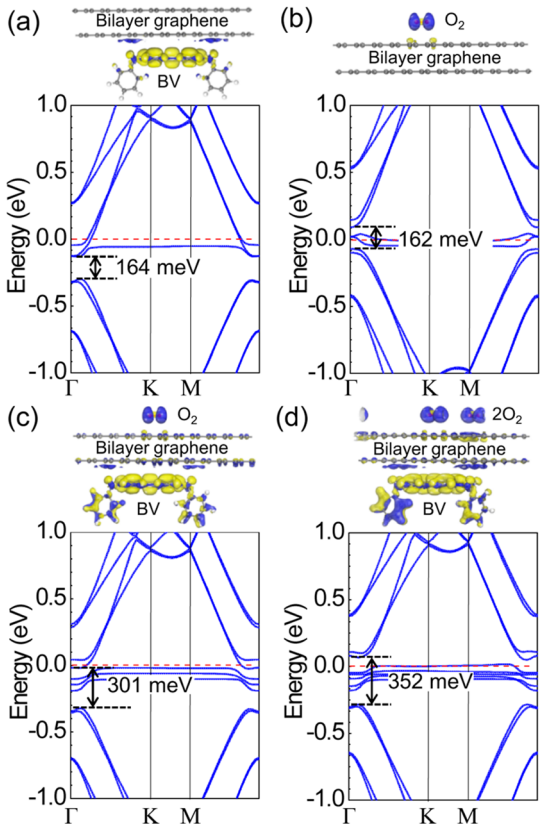

Figure 4. Induced charge distribution (top panel) and band structure (bottom panel) of one-side-doped bilayer graphene by individual (a) BV and (b) O_2 and dual-side-doped bilayer graphene by (c) O_2/BV and (d) $2O_2$/BV. The blue and yellow colors indicate the accumulation and depletion of electrons, respectively. The induced band gap is indicated in the band structures.

on the graphene surface and impurities exist in the BV layer. Therefore, the doping states are less dispersed than those of our simulation results.

By utilizing the high on/off ratio and large hysteresis in our band-gap-opened bilayer grahene FET, we demonstrated nonvolatile memory behavior (Figure 5). The same device structure as shown in Figure 1 was used, and its schematic is illustrated in Figure 5a. p-Si was used as a control gate electrode, and BV was used as an n-type dopant as well as a charge trap layer. Organic molecules have been widely used as a charge trap layer for memory transistors due to their low cost, easy processability, and structural flexibility.[30] The memory behavior of a bilayer graphene FET was measured when the V_{CNP} (forward sweep) reached around 0 V because this state provides the highest on/off ratio at the read gate bias (V_{GS} = 0 V), as indicated in Figure 5b (dotted line). We measured the memory hysteresis loop and memory window (ΔV_{CNP}) defined as the difference between two minimum conductance points (V_{CNP}) by modulating the amount of charges stored in the charge trap layer with different gate bias sweep ranges (Figure 5b). During the gate bias sweep from −70 to 70 V, no significant hysteresis is observed. However, the hysteresis increases as a higher gate bias is applied. By applying a gate bias from −150 to 150 V, ΔV_{CNP} increases up to 120 V. The two minimum V_{CNP} points from the forward and reverse gate bias sweeps are depicted in Figure 5c, and their differences (ΔV_{CNP}) are shown in the inset. The hysteresis mechanism of our device cannot be explained by a dipolar polarization of BV molecules because the direction of hysteresis in our device is opposite conventional ferroelectric gating.[31,32] Because a certain amount of charge transfer occurs by the dopants, as evidenced by the Fermi level shift (Figure 3), charges are accumulated on both sides of the graphene layers with different polarities. The accumulated charges may limit the current flow during gate voltage sweeping and provoke hysteresis.

The dynamic behavior of our device is shown in Figure 5d. We applied a gate voltage pulse of 150 V to program (high current level) and −150 V to erase (low current level) with a pulse width of 1 s on the control gate electrode. When the control gate bias returned to 0 V, we read the source−drain current states with a source−drain bias of 10 mV without applying a gate bias. The current is initially in the erased state, and it moves to the programmed state after applying a positive gate pulse (150 V, 1 s). It again shifts to the erased state with the application of an opposite gate pulse (−150 V, 1 s). Clear programmed and erased states are observed, demonstrating that our memory device works properly. The control gate bias can be reduced by replacing the 300 nm SiO_2 by a thinner or high-*k* dielectric layer (see Supporting Information Figure S4).[33] We also tested a shorter gate pulse of 100 ms (see Supporting Information Figure S5a), which also revealed clear current switching states while the programmed/erased current level was lower. This may originate from the insufficient capture and release time of the trap charges in the BV layer, which can be explained by the sweep-rate-dependent measurements (see Supporting Information Figure S5b).[34] As a result, large gate pulse time is required for our device to achieve a large memory window as well as a high programmed/erased current ratio.

The device stability was further investigated by conducting a retention time test at a constant source−drain bias of 10 mV (Figure 5e). The device is programmed by applying a positive gate pulse (150 V, 5 s) and erased by applying a negative gate pulse (−150 V, 5 s). It is important to note that the initial current ratio between the programmed and erased states is 34.5, which is remarkably higher than values obtained in previous reports (~4).[12] The current ratio is maintained above a value of 10 even after 10^4 s. In Figure 5f, the program/erase current ratio of our memory device as a function of the retention time is compared with those obtained in previous reports in which the channel of the FET is composed of graphene. Compared to

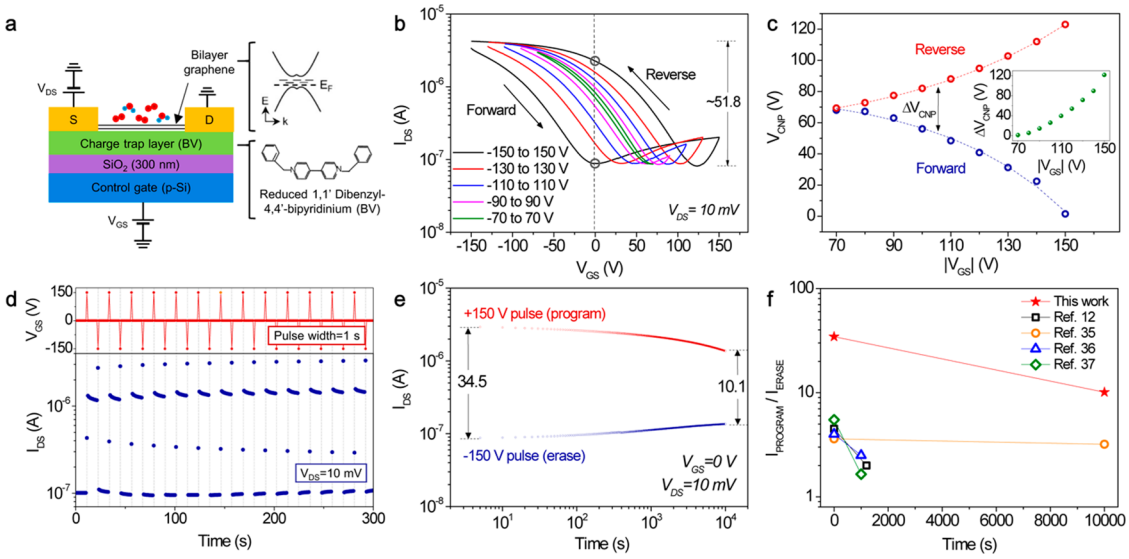

Figure 5. (a) Schematic of a nonvolatile memory cell with a bilayer graphene channel and source/drain electrodes on BV/SiO_2 (300 nm)/Si. The band gap of bilayer graphene is opened by dual-side doping with BV and atmospheric dopants. Si is used as a control gate, and BV is used as an n-type dopant as well as a charge trap layer. (b) Memory hysteresis loops of a bilayer graphene FET (on/off ratio of ~51.8) with different control gate biases where a V_{DS} of 10 mV was applied. (c) V_{CNP} shifts as a function of the applied control gate bias with different sweep directions (reverse: red color, forward: blue color). The memory window (ΔV_{CNP}) is shown in the inset. (d) Dynamic behavior of the memory transistor. The switching between the program and erase states was measured at V_{DS} = 10 mV with the application of control gate pulses (±150 V for 1 s). (e) Retention test with V_{DS} = 10 mV and V_{GS} = 0 V after application of a control gate pulse of 150 V (for program) and −150 V (for erase) for 5 s. (f) Comparison of the program/erase current ratio of our device as a function of the retention time as compared to the results of previous reports.

previous reports, the initial program/erase current ratio of our device is at least ~7.5 times higher and the ratio after 10^4 s is still larger. This is because in previous reports graphene FETs with low on/off ratio were utilized (less than 10).[12,35−37] Although our device requires a relatively high control gate bias and the speed is slow, the performance can be further improved by modifying the device geometries such as the thickness of the gate oxide. In addition, the p-type doping by atmospheric molecules may not sufficiently satisfy the industrial criteria of stability at this moment. Therefore, further study on developing a more durable doping method is necessary for the conventional circuit packaging.

CONCLUSIONS

In summary, we demonstrated that dual-side chemical doping can produce a local electric field to open the band gap of bilayer graphene. By controlling the concentration of both n-type and p-type dopants, we modulated the band gap and obtained a high on/off ratio of a bilayer graphene FET of up to 76.1 and a mobility of ~3100 $cm^2 V^{-1} s^{-1}$ without degradation of the on-current. This can be mainly attributed to physisorbed dopants without provoking sp^3 structural disorders. Using BV as a charge trap layer, we successfully demonstrated nonvolatile memory behavior of the band-gap-opened bilayer graphene FET. Due to the sufficiently opened band gap in graphene, the program/erase current ratio of the memory device was much higher than that obtained in previous reports. For the first time, our study demonstrates the potential use of a high on/off ratio graphene FET for memory applications. By integrating with a flexible substrate and dielectric,[33] our device will be useful as an element for flexible, transparent, and wearable electronics.

EXPERIMENTAL SECTION

Preparation of the BV Layer on SiO_2/Si. The 0.245 g of benzyl viologen powder (benzyl viologen dichloride 97%, Sigma-Aldrich) was dissolved in 15 mL of deionized water to obtain a 40 mM BV solution. Then, 15 mL of toluene (Sigma-Aldrich) was added into the deionized water solution containing benzyl viologen, resulting in a biphasic solution. Benzyl viologen in deionized water was reduced by adding 3 g of sodium borohydride (powder ≥98%, Sigma-Aldrich) as a catalytic reducing agent, and the reduced benzyl viologen was transferred from the water phase to the toluene phase. The resulting solution was maintained for 2 days. The toluene phase was dropped onto a SiO_2 (300 nm)/Si wafer at 7000 rpm for 60 s.

Fabrication of Dual-Side-Doped Bilayer Graphene. A bilayer graphene flake was prepared on the BV/SiO_2/Si wafer by mechanical exfoliation from natural Kish graphite (grade 300, Graphene Supermarket) by the Scotch tape method. The position and thickness of the graphene flake were identified by optical microscopy and Raman spectroscopy, respectively. The carbon grid of the TEM grid (STEM150 Cu, Okenshoji) was removed by oxygen plasma followed by fixing the TEM grid onto the graphene flake. Cr/Au (5 nm/70 nm) was evaporated by an e-beam/thermal evaporator to pattern the source and drain

electrodes. The sample was kept in air to dope the top of bilayer graphene by atmospheric dopants (humidity ~27%).

Measurements. Raman spectroscopy (RM1000 microprobe, Renishaw) was used to characterize the graphene. A vacuum probe station system (M5VC, MS Tech) and semiconductor characterization system (4200-SCS, Keithley) were used for the *I*−*V* and *C*−*V* measurements. A precision source/measure unit (B2902A, Agilent) was used to measure the memory behavior. AFM (SPA400, Seiko) was used to measure the roughness and thickness of the BV layer.

Conflict of Interest: The authors declare no competing financial interest.

Supporting Information Available: The Supporting Information is available free of charge on the ACS Publications website at DOI: 10.1021/acsnano.5b03130.

Supplementary text and Figures S1 to S5 (PDF)

Acknowledgment. This work was supported by the Institute for Basic Science (IBS-R011-D1) and by the Human Resources Development program (No. 20124010203270) of the Korea Institute of Energy Technology Evaluation and Planning (KETEP) grant funded by the Korea government Ministry of Trade, Industry and Energy. The work at Harvard was supported by the NSF under DMR 1435487.

REFERENCES AND NOTES

1. Novoselov, K. S.; Geim, A. K.; Morozov, S. V.; Jiang, D.; Katsnelson, M. I.; Grigorieva, I. V.; Dubonos, S. V.; Firsov, A. A. Two-Dimensional Gas of Massless Dirac Fermions in Graphene. *Nature* **2005**, *438*, 197–200.
2. Zhang, Y.; Tan, Y.-W.; Stormer, H. L.; Kim, P. Experimental Observation of the Quantum Hall Effect and Berry's Phase in Graphene. *Nature* **2005**, *438*, 201–204.
3. Katsnelson, M. I.; Novoselov, K. S.; Geim, A. K. Chiral Tunnelling and the Klein Paradox in Graphene. *Nat. Phys.* **2006**, *2*, 620–625.
4. Dean, C. R.; Young, A. F.; Meric, I.; Lee, C.; Wang, L.; Sorgenfrei, S.; Watanabe, K.; Taniguchi, T.; Kim, P.; Shepard, K. L.; et al. Boron Nitride Substrates for High-Quality Graphene Electronics. *Nat. Nanotechnol.* **2010**, *5*, 722–726.
5. Yang, H.; Heo, J.; Park, S.; Song, H. J.; Seo, D. H.; Byun, K.-E.; Kim, P.; Yoo, I.; Chung, H.-J.; Kim, K. Graphene Barristor, a Triode Device with a Gate-Controlled Schottky Barrier. *Science* **2012**, *336*, 1140–1143.
6. Bae, S.; Kim, H.; Lee, Y.; Xu, X.; Park, J.-S.; Zheng, Y.; Balakrishnan, J.; Lei, T.; Kim, H. R.; Song, Y. I.; et al. Roll-to-Roll Production of 30-Inch Graphene Films for Transparent Electrodes. *Nat. Nanotechnol.* **2010**, *5*, 574–578.
7. Chae, S. J.; Günes, F.; Kim, K. K.; Kim, E. S.; Han, G. H.; Kim, S. M.; Shin, H.-J.; Yoon, S.-M.; Choi, J.-Y.; Park, M. H.; et al. Synthesis of Large-Area Graphene Layers on Poly-Nickel Substrate by Chemical Vapor Deposition: Wrinkle Formation. *Adv. Mater.* **2009**, *21*, 2328–2333.
8. Liao, L.; Lin, Y.-C.; Bao, M.; Cheng, R.; Bai, J.; Liu, Y.; Qu, Y.; Wang, K. L.; Huang, Y.; Duan, X. High-Speed Graphene Transistors with a Self-Aligned Nanowire Gate. *Nature* **2010**, *467*, 305–308.
9. Kim, B. J.; Lee, S.-K.; Kang, M. S.; Ahn, J.-H.; Cho, J. H. Coplanar-Gate Transparent Graphene Transistors and Inverters on Plastic. *ACS Nano* **2012**, *6*, 8646–8651.
10. Yun, J. M.; Park, S.; Hwang, Y. H.; Lee, E.-S.; Maiti, U.; Moon, H.; Kim, B.-H.; Bae, B.-S.; Kim, Y.-H.; Kim, S. O. Complementary p- and n-type Polymer Doping for Ambient Stable Graphene Inverter. *ACS Nano* **2014**, *8*, 650–656.
11. Kim, S. M.; Song, E. B.; Lee, S.; Zhu, J.; Seo, D. H.; Mecklenburg, M.; Seo, S.; Wang, K. L. Transparent and Flexible Graphene Charge-Trap Memory. *ACS Nano* **2012**, *6*, 7879–7884.
12. Choi, M. S.; Lee, G.-H.; Yu, Y.-J.; Lee, D.-Y.; Lee, S. H.; Kim, P.; Hone, J.; Yoo, W. J. Controlled Charge Trapping by Molybdenum Disulphide and Graphene in Ultrathin Heterostructured Memory Devices. *Nat. Commun.* **2013**, *4*, 1624.
13. Li, X.; Wang, X.; Zhang, L.; Lee, S.; Dai, H. Chemically Derived, Ultrasmooth Graphene Nanoribbon Semiconductors. *Science* **2008**, *319*, 1229–1232.
14. Wang, X.; Ouyang, Y.; Li, X.; Wang, H.; Guo, J.; Dai, H. Room-Temperature All-Semiconducting Sub-10 nm Graphene Nanoribbon Field Effect Transistors. *Phys. Rev. Lett.* **2008**, *100*, 206803.
15. Zhang, Y.; Tang, T.-T.; Girit, C.; Hao, Z.; Martin, M. C.; Zettl, A.; Crommie, M. F.; Shen, Y. R.; Wang, F. Direct Observation of a Widely Tunable Bandgap in Bilayer Graphene. *Nature* **2009**, *459*, 820–823.
16. Xia, F.; Farmer, D. B.; Lin, Y.-M.; Avouris, P. Graphene Field-Effect Transistors with High On/Off Current Ratio and Large Transport Band Gap at Room Temperature. *Nano Lett.* **2010**, *10*, 715–718.
17. Mak, K. F.; Lui, C. H.; Shan, J.; Heinz, T. F. Observation of an Electric-Field-Induced Band Gap in Bilayer Graphene by Infrared Spectroscopy. *Phys. Rev. Lett.* **2009**, *102*, 256405.
18. Park, J.; Jo, S. B.; Yu, Y.-J.; Kim, Y.; Yang, J. W.; Lee, W. H.; Kim, H. H.; Hong, B. H.; Kim, P.; Cho, K.; et al. Single-Gate Bandgap Opening of Bilayer Graphene by Dual Molecular Doping. *Adv. Mater.* **2012**, *24*, 407–411.
19. Duong, D. L.; Lee, S. M.; Chae, S. H.; Ta, Q. H.; Lee, S. Y.; Han, G. H.; Bae, J. J.; Lee, Y. H. Band-Gap Engineering in Chemically Conjugated Bilayer Graphene: *Ab initio* Calculations. *Phys. Rev. B: Condens. Matter Mater. Phys.* **2012**, *85*, 205413.
20. Wang, T. H.; Zhu, Y. F.; Jiang, Q. Towards Single-Gate Field Effect Transistor Utilizing Dual-Doped Bilayer Graphene. *Carbon* **2014**, *77*, 431–441.
21. Yang, J. W.; Lee, G.; Kim, J. S.; Kim, K. S. Gap Opening of Graphene by Dual $FeCl_3$-Acceptor and K-Donor Doping. *J. Phys. Chem. Lett.* **2011**, *2*, 2577–2581.
22. Novoselov, K. S.; Fal'ko, V. I.; Colombo, L.; Gellert, P. R.; Schwab, M. G.; Kim, K. A Roadmap for Graphene. *Nature* **2012**, *490*, 192–200.
23. Luo, Z.; Yu, T.; Shang, J.; Wang, Y.; Lim, S.; Liu, L.; Gurzadyan, G. G.; Shen, Z.; Lin, J. Large-Scale Synthesis of Bi-Layer Graphene in Strongly Coupled Stacking Order. *Adv. Funct. Mater.* **2011**, *21*, 911–917.
24. Wei, P.; Liu, N.; Lee, H. R.; Adijanto, E.; Ci, L.; Naab, B. D.; Zhong, J. Q.; Park, J.; Chen, W.; Cui, Y.; et al. Tuning the Dirac Point in CVD-Grown Graphene Through Solution Processed n-Type Doping with 2-(2-Methoxyphenyl)-1,3-dimethyl-2,3-dihydro-1H-benzoimidazole. *Nano Lett.* **2013**, *13*, 1890–1897.
25. Zhang, W.; Lin, C.-T.; Liu, K.-K.; Tite, T.; Su, C.-Y.; Chang, C.-H.; Lee, Y.-H.; Chu, C.-W.; Wei, K.-H.; Kuo, J.-L.; et al. Opening an Electrical Band Gap of Bilayer Graphene with Molecular Doping. *ACS Nano* **2011**, *5*, 7517–7524.
26. Lin, S. S.; Chen, B. G.; Pan, C. T.; Hu, S.; Tian, P.; Tong, L. M. Unintentional Doping Induced Splitting of G Peak in Bilayer Graphene. *Appl. Phys. Lett.* **2011**, *99*, 233110.
27. Wang, H.; Wu, Y.; Cong, C.; Shang, J.; Yu, T. Hysteresis of Electronic Transport in Graphene Transistors. *ACS Nano* **2010**, *4*, 7221–7228.
28. Ryu, S.; Liu, L.; Berciaud, S.; Yu, Y.-J.; Liu, H.; Kim, P.; Flynn, G. W.; Brus, L. E. Atmospheric Oxygen Binding and Hole Doping in Deformed Graphene on a SiO_2 Substrate. *Nano Lett.* **2010**, *10*, 4944–4951.
29. Szafranek, B. N.; Schall, D.; Otto, M.; Neumaier, D.; Kurz, H. High On/Off Ratios in Bilayer Graphene Field Effect Transistors Realized by Surface Dopants. *Nano Lett.* **2011**, *11*, 2640–2643.
30. Chou, Y.-H.; Takasugi, S.; Goseki, R.; Ishizone, T.; Chen, W.-C. Nonvolatile Organic Field-Effect Transistor Memory Devices Using Polymer Electrets with Different Thiophene Chain Lengths. *Polym. Chem.* **2014**, *5*, 1063–1071.
31. Zheng, Y.; Ni, G.-X.; Toh, C.-T.; Tan, C.-Y.; Yao, K.; Özyilmaz, B. Graphene Field-Effect Transistors with Ferroelectric Gating. *Phys. Rev. Lett.* **2010**, *105*, 166602.
32. Egginger, M.; Bauer, S.; Schwödiauer, R.; Neugebauer, H.; Sariciftci, N. S. Current versus Gate Voltage Hysteresis in Organic Field Effect Transistors. *Monatsh. Chem.* **2009**, *140*, 735–750.
33. Chae, S. H.; Yu, W. J.; Bae, J. J.; Duong, D. L.; Perello, D.; Jeong, H. Y.; Ta, Q. H.; Ly, T. H.; Vu, Q. A.; Yun, M.; et al. Transferred Wrinkled Al_2O_3 for Highly Stretchable and

Transparent Graphene–Carbon Nanotube Transistors. *Nat. Mater.* **2013**, *12*, 403–409.
34. Jin, S. H.; Islam, A. E.; Kim, T.-I.; Kim, J.-H.; Alam, M. A.; Rogers, J. A. Sources of Hysteresis in Carbon Nanotube Field-Effect Transistors and Their Elimination *Via* Methylsiloxane Encapsulants and Optimized Growth Procedures. *Adv. Funct. Mater.* **2012**, *22*, 2276–2284.
35. Jang, S.; Hwang, E.; Cho, J. H. Graphene Nano-Floating Gate Transistor Memory on Plastic. *Nanoscale* **2014**, *6*, 15286–15292.
36. Song, E. B.; Lian, B.; Kim, S. M.; Lee, S.; Chung, T.-K.; Wang, M.; Zeng, C.; Xu, G.; Wong, K.; Zhou, Y.; et al. Robust Bi-Stable Memory Operation in Single-Layer Graphene Ferroelectric Memory. *Appl. Phys. Lett.* **2011**, *99*, 042109.
37. Imam, S. A.; Deshpande, T.; Guermoune, A.; Siaj, M.; Szkopek, T. Charge Transfer Hysteresis in Graphene Dual-Dielectric Memory Cell Structures. *Appl. Phys. Lett.* **2011**, *99*, 082109.